iScience

CellPress
OPEN ACCESS

Article

Rapid spread of the SARS-CoV-2 JN.1 lineage is associated with increased neutralization evasion

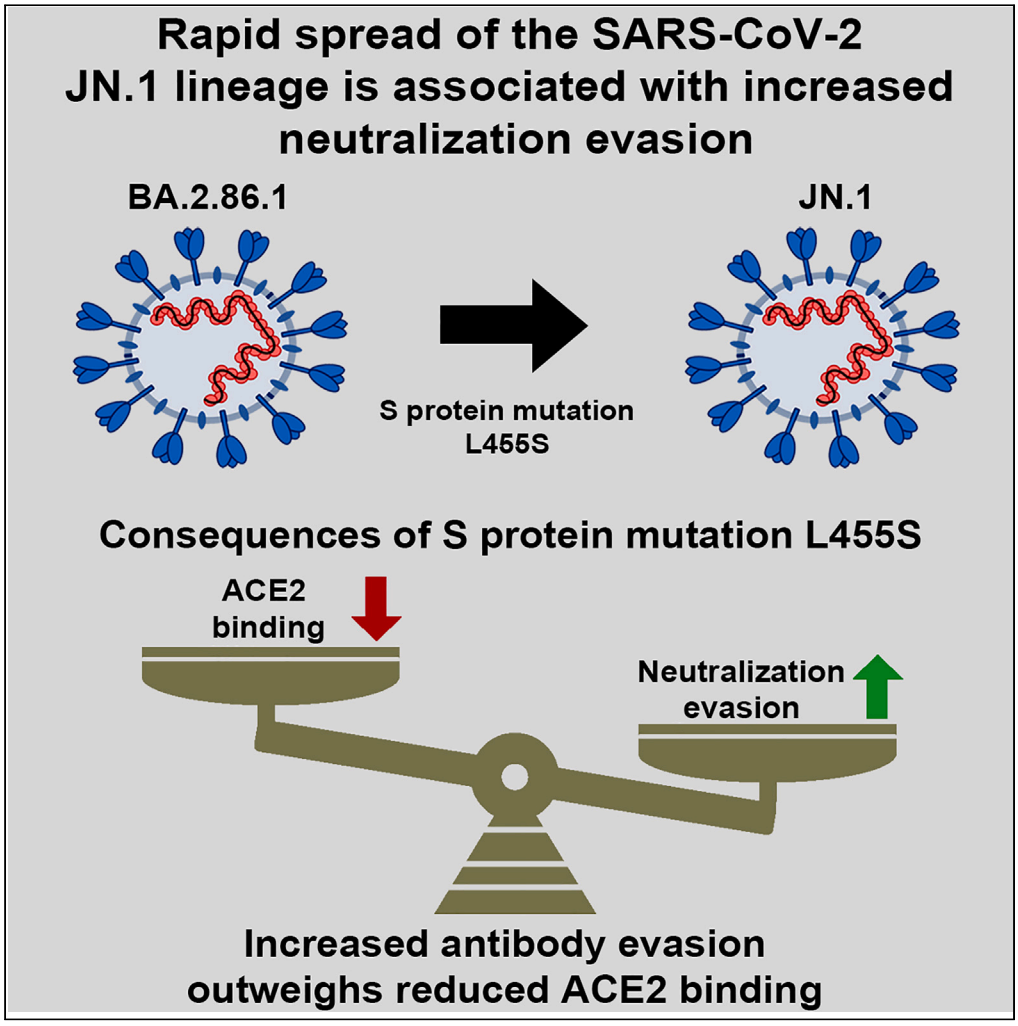

Lu Zhang, Alexandra Dopfer-Jablonka, Anne Cossmann, ..., Georg M.N. Behrens, Stefan Pöhlmann, Markus Hoffmann

mhoffmann@dpz.eu

Highlights

Rapid spread of the SARS-CoV-2 JN.1 lineage is linked to S protein mutation L455S

Mutation L455S reduces S protein-driven cell entry

Diminished cell entry is linked to reduced ACE2 binding efficiency

Mutation L455S leads to increased neutralization resistance

Zhang et al., iScience 27, 109904
June 21, 2024
https://doi.org/10.1016/j.isci.2024.109904

iScience

CellPress
OPEN ACCESS

Article

Rapid spread of the SARS-CoV-2 JN.1 lineage is associated with increased neutralization evasion

Lu Zhang,[1,2] Alexandra Dopfer-Jablonka,[3,4] Anne Cossmann,[3] Metodi V. Stankov,[3] Luise Graichen,[1,2] Anna-Sophie Moldenhauer,[1] Christina Fichter,[5] Anupriya Aggarwal,[5] Stuart G. Turville,[5] Georg M.N. Behrens,[3,4,6] Stefan Pöhlmann,[1,2] and Markus Hoffmann[1,2,7,*]

SUMMARY

In July/August 2023, the highly mutated severe acute respiratory syndrome coronavirus 2 (SARS-CoV-2) BA.2.86 lineage emerged and its descendant JN.1 is on track to become the dominant SARS-CoV-2 lineage globally. Compared to the spike (S) protein of the parental BA.2.86 lineage, the JN.1 S protein contains one mutation, L455S, which may affect receptor binding and antibody evasion. Here, we performed a virological assessment of the JN.1 lineage employing pseudovirus particles bearing diverse SARS-CoV-2 S proteins. Using this strategy, it was found that S protein mutation L455S confers increased neutralization resistance but reduces ACE2 binding capacity and S protein-driven cell entry efficiency. Altogether, these data suggest that the benefit of increased antibody evasion outweighs the reduced ACE2 binding capacity and further enabled the JN.1 lineage to effectively spread in the human population.

INTRODUCTION

While the transition of the coronavirus disease 2019 (COVID-19) from a pandemic to an endemic state is ongoing, the causative agent, severe acute respiratory syndrome coronavirus 2 (SARS-CoV-2), continues to circulate globally. Viruses belonging to different XBB-sublineages were highly prevalent in most of 2023 (Figure 1A) and independently acquired identical mutations, a phenomenon called convergent evolution, suggesting a constrained evolutionary space for XBB-sublineages. Hence, the emergence of the highly divergent BA.2.86 lineage in July/August 2023, which is reminiscent of the emergence of the Omicron variant in late 2021, represents a significant advance in SARS-CoV-2 evolution. Compared to the spike (S) protein of the parental BA.2 lineage, the BA.2.86 S protein harbors over 30 mutations. Recent studies demonstrated that BA.2.86 efficiently binds to ACE2 and evades neutralization by vaccination- and infection-induced antibodies with high efficiency, although neutralization evasion did not exceed that of co-circulating XBB-sublineages.[1–6] However, the BA.2.86 sublineage JN.1, which was first detected in Europe in August/September 2023, is on track to become the dominant SARS-CoV-2 lineage globally (Figure 1A) and has been classified as a variant of interest by the World Health Organization.[7] The JN.1 S protein contains one mutation, L455S, compared to BA.2.86 S protein, which resides in the receptor binding domain (RBD) and thus may modulate cell entry efficiency and neutralization sensitivity (Figures 1B and 1C).

Here, we performed an initial virological assessment of the JN.1 lineage, using S protein-bearing pseudovirus particles ($_{pp}$), which represent an adequate surrogate model to study SARS-CoV-2 entry and neutralization.[8]

RESULTS

The S protein of JN.1 displays reduced cell entry and ACE2 binding capacities compared to the S protein of BA.2.86.1

We first analyzed the ability of the JN.1 S protein to drive cell entry. Particles bearing JN.1 S protein (JN.1$_{pp}$) were used to infect Vero (African green monkey, kidney), Vero-TMPRSS2 (Vero cells overexpressing TMPRSS2), Vero-ACE2+TMPRSS2 (Vero cells overexpressing ACE2 and TMPRSS2), 293T (human, kidney), and Calu-3 cells (human, lung), which are commonly used for SARS-CoV-2 research. For comparison, we included particles bearing the S protein of the B.1 lineage (B.1$_{pp}$, used as reference), which circulated in the early phase of the pandemic, or the S proteins of BA.2.86.1 (which has identical S protein mutations as BA.2.86; BA.2.86.1$_{pp}$) or contemporary XBB-sublineages, XBB.1.5

[1]Infection Biology Unit, German Primate Center, Göttingen, Germany
[2]Faculty of Biology and Psychology, Georg-August-University Göttingen, Göttingen, Germany
[3]Department of Rheumatology and Immunology, Hannover Medical School, Hannover, Germany
[4]German Center for Infection Research (DZIF), Partner Site Hannover-Braunschweig, Hannover, Germany
[5]The Kirby Institute, University of New South Wales, Sydney, NSW, Australia
[6]Center for Individualized Infection Medicine (CiiM), Hannover, Germany
[7]Lead contact
*Correspondence: mhoffmann@dpz.eu
https://doi.org/10.1016/j.isci.2024.109904

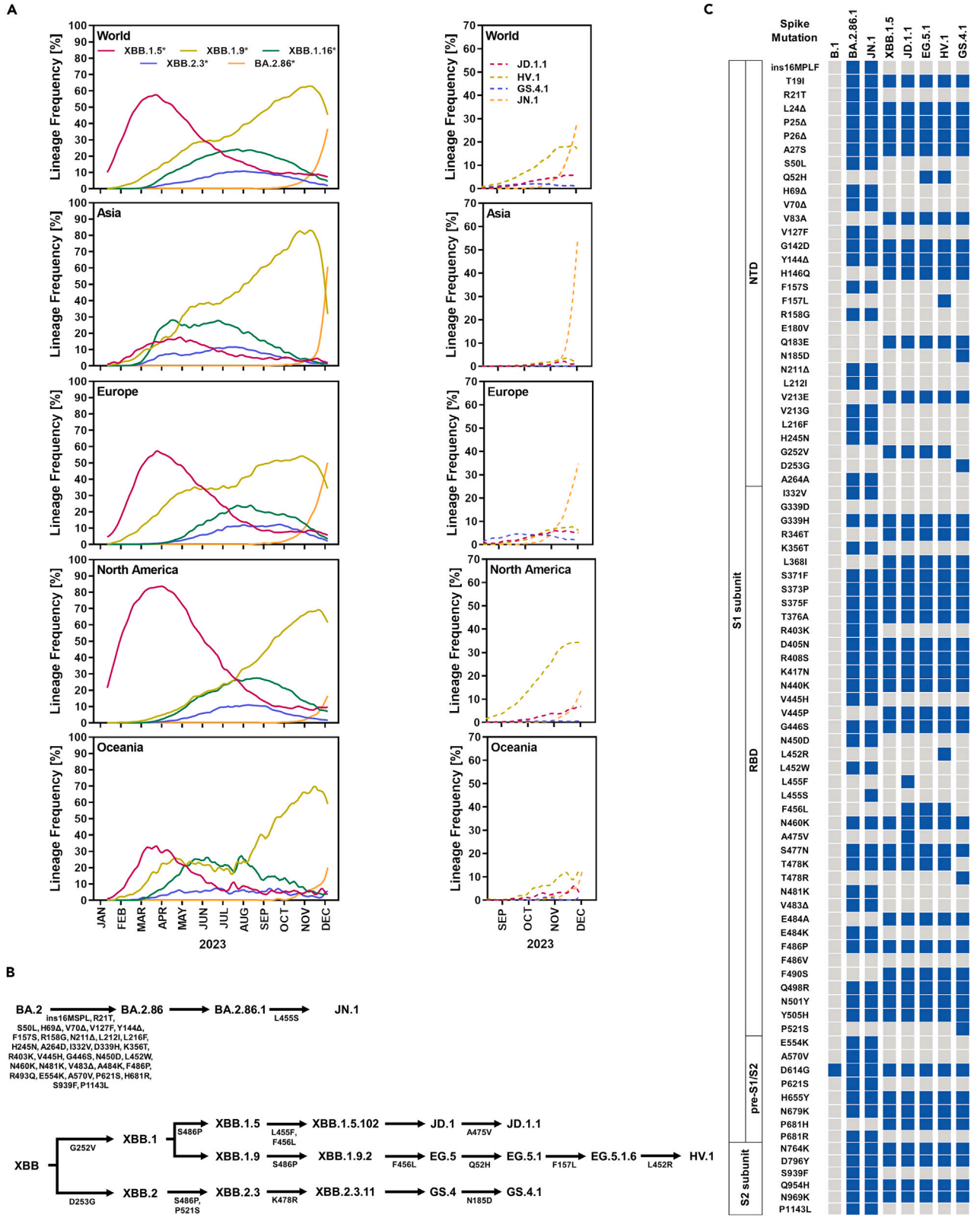
A
World
XBB.1.5*
XBB.1.9*
XBB.1.16*
XBB.2.3*
BA.2.86*
JD.1.1
HV.1
GS.4.1
JN.1
Asia
Europe
North America
Oceania
Lineage Frequency [%]
JAN
FEB
MAR
APR
MAY
JUN
JUL
AUG
SEP
OCT
NOV
DEC
2023
B
BA.2
ins16MSPL, R21T, S50L, H69Δ, V70Δ, V127F, Y144Δ, F157S, R158G, N211Δ, L212I, L216F, H245N, A264D, I332V, D339H, K356T, R403K, V445H, G446S, N450D, L452W, N460K, N481K, V483Δ, A484K, F486P, R493Q, E554K, A570V, P621S, H681R, S939F, P1143L
BA.2.86
BA.2.86.1
L455S
JN.1
XBB
G252V
XBB.1
S486P
XBB.1.5
L455F, F456L
XBB.1.5.102
JD.1
A475V
JD.1.1
XBB.1.9
S486P
XBB.1.9.2
F456L
EG.5
Q52H
EG.5.1
F157L
EG.5.1.6
L452R
HV.1
D253G
XBB.2
S486P, P521S
XBB.2.3
K478R
XBB.2.3.11
GS.4
N185D
GS.4.1
C
Spike Mutation
B.1
BA.2.86.1
JN.1
XBB.1.5
JD.1.1
EG.5.1
HV.1
GS.4.1
S1 subunit
S2 subunit
NTD
RBD
pre-S1/S2
ins16MPLF
T19I
R21T
L24Δ
P25Δ
P26Δ
A27S
S50L
Q52H
H69Δ
V70Δ
V83A
V127F
G142D
Y144Δ
H146Q
F157S
F157L
R158G
E180V
Q183E
N185D
N211Δ
L212I
V213E
V213G
L216F
H245N
G252V
D253G
A264A
I332V
G339D
G339H
R346T
K356T
L368I
S371F
S373P
S375F
T376A
R403K
D405N
R408S
K417N
N440K
V445H
V445P
G446S
N450D
L452R
L452W
L455F
L455S
F456L
N460K
A475V
S477N
T478K
T478R
N481K
V483Δ
E484A
E484K
F486P
F486V
F490S
Q498R
N501Y
Y505H
P521S
E554K
A570V
D614G
P621S
H655Y
N679K
P681H
P681R
N764K
D796Y
S939F
Q954H
N969K
P1143L

Figure 1. Emergence and rapid spread of the SARS-CoV-2 JN.1 lineage

(A) Frequencies of major SARS-CoV-2 lineages (left panels) in 2023 and trends for selected SARS-CoV-2 sublineages in late 2023 (right panels) on a global scale and for selected continents (Asia, Europe, North America, and Oceania). Graphs were generated using a seven-day sliding window and are based on data retrieved from https://cov-spectrum.org/ on 18.12.2023. Lineages suffixed with an asterisk (*) also include their respective sublineages.

(B) Recent trends in the evolution of SARS-CoV-2 BA.2 and XBB-sublineages. Evolutionary steps leading to JN.1 and XBB-sublineages JD.1.1, HV.1, and GS.4.1. S protein mutations are indicated.

(C) S protein mutations (blue boxes) of B.1, BA.2.86.1, JN.1, XBB.1.5, JD.1.1, EG.5.1, HV.1, and GS.4.1 compared to the Wuhan-Hu-01 isolate (gray boxes indicate non-mutated residues). Abbreviations: NTD, N-terminal domain; RBD, receptor-binding domain, pre-S1/S2, region between RBD and S1/S2 cleavage site.

(XBB.1.5$_{pp}$), JD.1.1 (JD.1.1$_{pp}$), EG.5.1 (EG.5.1$_{pp}$), HV.1 (HV.1$_{pp}$), and GS.4.1 (GS.4.1$_{pp}$). All S proteins under study were efficiently cleaved and incorporated into pseudoviruses without significant differences (Figures S1A–S1C). For Vero, Vero-TMPRSS2, and Vero-ACE2-TMPRSS2 cells, no major differences in entry efficiency were observed between the different pseudoviruses. However, it was noticed that Vero cell entry by B.1$_{pp}$ was slightly reduced as compared to the other pseudoviruses, while the opposite trend was seen for Vero-TMPRSS2 and Vero-ACE2-TMPRSS2 cells (Figure 2A). Entry of XBB.1.5$_{pp}$, JD.1.1$_{pp}$, EG.5.1$_{pp}$, HV.1$_{pp}$, BA.2.86.1$_{pp}$, and JN.1$_{pp}$ into 293T cells was increased compared to B.1$_{pp}$, whereas GS.4.1$_{pp}$ entry was comparable to B.1$_{pp}$ (Figure 2A). For Calu-3 cells, which endogenously express TMPRSS2 and thus allow for SARS-CoV-2 entry at the plasma membrane, we observed substantially reduced cell entry efficiencies for XBB.1.5$_{pp}$, JD.1.1$_{pp}$, EG.5.1$_{pp}$, HV.1$_{pp}$, GS.4.1$_{pp}$, and JN.1$_{pp}$ compared to B.1$_{pp}$. In contrast, BA.2.86.1$_{pp}$ entered Calu-3 cells with similar efficiency as B.1$_{pp}$ (Figure 2A), which is in line with the findings of two recent studies.[5,6] When entry efficiencies of BA.2.86.1$_{pp}$ and JN.1$_{pp}$ were compared, it was noted that for three out of five cell lines tested the latter showed reduced entry capacity.

We next assessed ACE2 binding efficiency. Using ACE2 binding by the B.1 S protein as reference, we found that all BA.2.86- and XBB-sublineage S proteins displayed augmented ACE2 binding capacity, with the exception of the GS.4.1 S protein (Figure 2B). Further, ACE2 binding by the JN.1 S protein was reduced as compared to BA.2.86.1 S protein (Figure 2B).

Particles bearing the S protein of JN.1 show augmented neutralization resistance compared to particles bearing BA.2.86.1 S protein

Finally, we studied the neutralization sensitivity of JN.1$_{pp}$ to antibodies induced upon vaccination or vaccination plus infection. Our first cohort included individuals without SARS-CoV-2 infection, who recently received the XBB.1.5-adapted mRNA booster vaccine of Pfizer-BioNTech (Table S1). All plasma samples displayed highest neutralizing activity against B.1$_{pp}$ (geometric mean titer [GMT] = 2,833), followed by XBB.1.5$_{pp}$ (GMT = 931), JD.1.1$_{pp}$ (GMT = 505), GS.4.1$_{pp}$ (GMT = 373), BA.2.86.1$_{pp}$ (GMT = 307), EG.5.1$_{pp}$ (GMT = 259), HV.1$_{pp}$ (GMT = 199), and JN.1$_{pp}$ (GMT = 139). Notably, JN.1$_{pp}$ neutralization was 2.5-fold reduced as compared to BA.2.86.1$_{pp}$ (Figure 2C). We extended our analysis to plasma from XBB.1.5-adapted mRNA vaccine-boostered individuals that had a SARS-CoV-2 infection between January 2022 and March 2023 (Table S1). Here, neutralization activity was highest for B.1$_{pp}$ (GMT = 6,734), followed by GS.4.1$_{pp}$ (GMT = 3,904), BA.2.86.1$_{pp}$ (GMT = 3,568), XBB.1.5$_{pp}$ (GMT = 2,927), EG.5.1$_{pp}$ (GMT = 2,667), HV.1$_{pp}$ (GMT = 1,970), JN.1$_{pp}$ (GMT = 1,582), and JD.1.1$_{pp}$ (GMT = 1,466). Neutralization of JN.1$_{pp}$ was again 2.5-fold lower as compared to BA.2.86.1$_{pp}$ neutralization (Figure 2C).

DISCUSSION

Collectively, our findings demonstrate that JN.1 has developed heightened resistance to neutralization through acquisition of S protein mutation L455S, confirming and expanding upon previous research.[9–11] While increased neutralization resistance came at the cost of suboptimal ACE2 binding, the current increase in JN.1 prevalence suggests that the benefit of increased antibody evasion outweighs the reduced ACE2 binding capacity. In this context it should be noted that some viruses within the JN.1 lineages already acquired an additional S protein mutation (i.e., T572I) that is predicted to improve ACE2 binding by modulating the conformation of the RBD[12] and thus may further boost infectivity and transmissibility.

Of note, while our study did not reveal major differences in Vero and Vero-TMPRSS2 cell entry of pseudoviruses bearing B.1, XBB.1.5, or BA.2.86.1 S proteins, two recent studies reported attenuated spread of authentic XBB.1.5 and BA.2.86/BA.2.86.1 in Vero E6 and Vero E6-TMPRSS2 cells as compared to viruses from the early phase of the pandemic that harbor only the D614G mutation in their S protein (e.g., B.1),[4,11] indicating that mutations in viral proteins other than the S protein might modulate infectivity. In addition, a recent study using authentic BA.2.86 and JN.1 came to the conclusion that increased neutralization escape may not be the reason for the recent upsurge in JN.1 incidence.[13] Altogether, these contrasting findings highlight that more research on the biological traits of XBB sublineages BA.2.86 and JN.1 is needed.

Limitations of the study

The following limitations apply to our study. First, we utilized pseudovirus particles for the present study and although these particles have been shown to adequately recapitulate SARS-CoV-2 cell entry and its inhibition,[8,14] some of our results await formal confirmation with authentic SARS-CoV-2 lineages. Second, since we employed cell lines for the analysis of S protein-driven host cell entry of SARS-CoV-2 lineages, our studies should be extended to primary cell culture models, organoid cultures and *in vivo* models. Third, with respect to the *in vitro* neutralization data, it needs to be stated that due to the small sample size for the two cohorts, it was not possible to conduct an analysis on the potential impact of biological factors (e.g., age, gender, or comorbidities) on neutralization efficiency. Fourth, all plasma samples were

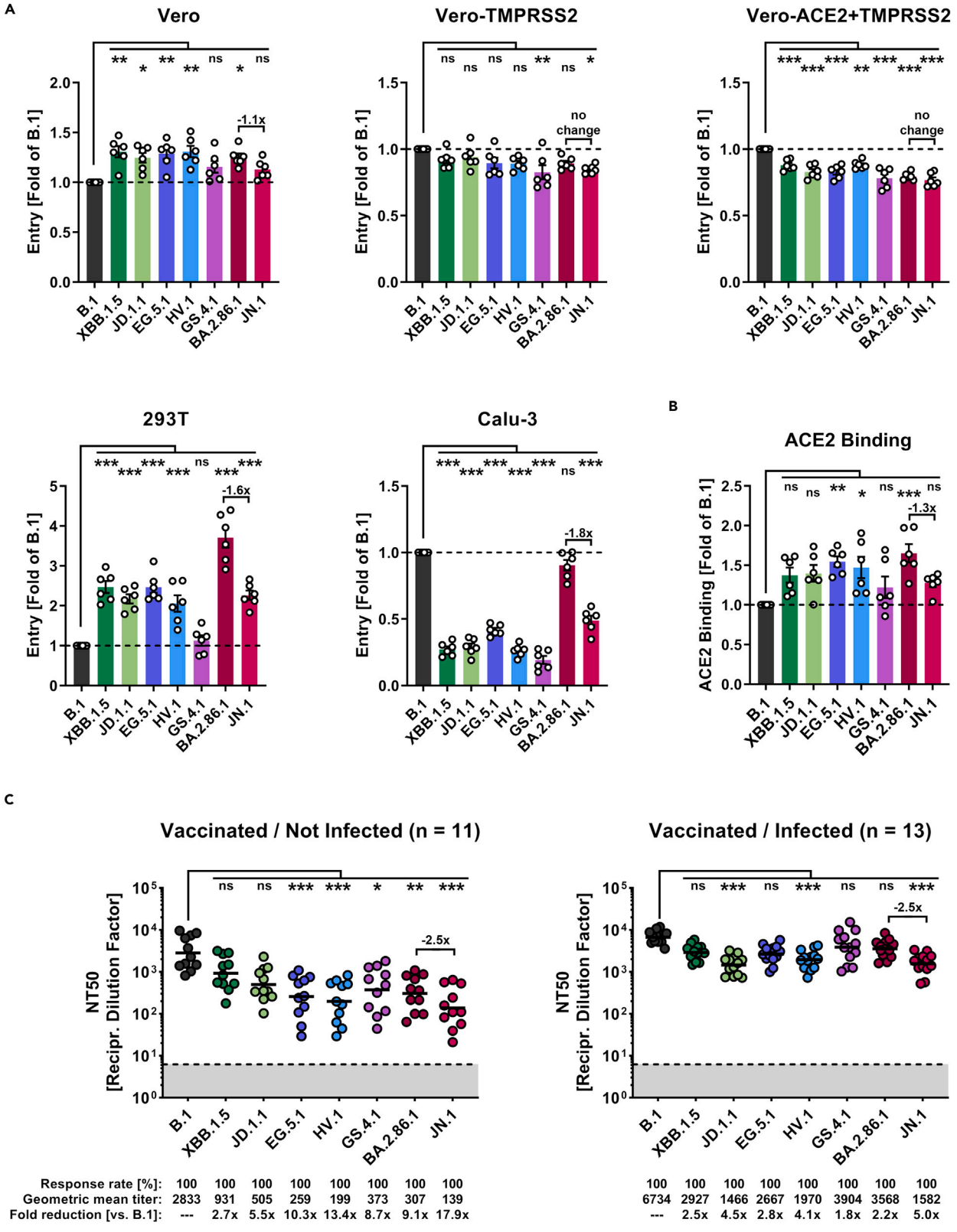
A
Vero
Vero-TMPRSS2
Vero-ACE2+TMPRSS2
293T
Calu-3
Entry [Fold of B.1]
-1.1x
no change
-1.6x
-1.8x
B
ACE2 Binding
ACE2 Binding [Fold of B.1]
-1.3x
B.1
XBB.1.5
JD.1.1
EG.5.1
HV.1
GS.4.1
BA.2.86.1
JN.1
C
Vaccinated / Not Infected (n = 11)
Vaccinated / Infected (n = 13)
NT50 [Recipr. Dilution Factor]
-2.5x
Response rate [%]: 100 100 100 100 100 100 100 100
Geometric mean titer: 2833 931 505 259 199 373 307 139
Fold reduction [vs. B.1]: --- 2.7x 5.5x 10.3x 13.4x 8.7x 9.1x 17.9x
100 100 100 100 100 100 100 100
6734 2927 1466 2667 1970 3904 3568 1582
--- 2.5x 4.5x 2.8x 4.1x 1.8x 2.2x 5.0x

Figure 2. Cell entry and neutralization sensitivity of the SARS-CoV-2 JN.1 lineage

(A) Entry efficiency of the JN.1 lineage. Pseudotype particles ($_{pp}$) harboring the indicated S proteins were inoculated onto the indicated cell lines and entry was analyzed. Presented are mean data from six biological replicates (four technical replicates), with cell entry normalized against particles harboring the B.1 S protein (=1). Error bars indicate the standard error of the mean (SEM). Further, the mean fold change in entry efficiency between BA.2.86.1$_{pp}$ and JN.1$_{pp}$ is indicated. See also Figure S1D.

(B) ACE2 binding efficiency of the JN.1 lineage. 293T cells transiently expressing the indicated S proteins were analyzed for ACE2 binding by flow cytometry. Presented are mean data from six biological replicates (single replicates), with ACE2 binding corrected for S protein cell surface expression and normalized against the B.1 S protein (=1). Error bars indicate the SEM. Further, the mean fold change in ACE2 binding between BA.2.86.1 and JN.1 is indicated. See also Figures S1E and S1F.

(C) Sensitivity of the JN.1 lineage to neutralization. Pseudotype particles harboring the indicated S proteins were incubated with plasma from vaccinated individuals without (n = 11; left) or with a history of SARS-CoV-2 infection (n = 13; right), before being inoculated onto Vero cells. Pseudovirus cell entry was normalized against samples without plasma (=0% inhibition). Presented are geometric mean titers (GMTs) from a single biological replicate (four technical replicates). Information below the graphs shows response rates (proportion of plasma samples with neutralizing activity), GMT, and median fold GMT change compared to B.1$_{pp}$. Further, the median fold change in neutralization between BA.2.86.1$_{pp}$ and JN.1$_{pp}$ is indicated. Please also see Table S1 and Figure S2. For (A) and (B), statistical significance was assessed by two-way analysis of variance with Tukey's multiple comparison test, while the Friedmann test with Dunn's multiple comparison test was used in (C) ($p > 0.05$, not significant [ns]; $p \leq 0.05$, *; $p \leq 0.01$, **; $p \leq 0.001$, ***).

collected within three weeks post XBB.1.5 booster vaccination, which is why we cannot make any statement on neutralization efficiency after an extended period of time. Fifth, for cohort 2 no information on the infecting SARS-CoV-2 lineage is available and patient-specific differences in the time intervals since the last infection may have an impact on SARS-CoV-2 lineage-specific neutralization efficiency. Sixth, given the possibility of an asymptomatic infection together with the decay dynamics of antibodies against viral antigens, we cannot rule out that some participants in the "vaccinated/not infected" group may have had an undocumented infection and nucleocapsid IgG levels may have decayed beneath the limit of detection at the time of testing. Seventh, neutralization sensitivity of the SARS-CoV-2 JN.1 lineage may vary with respect to cohorts with immune backgrounds distinct from those examined in this study. Finally, we did not test neutralization by therapeutic antibodies as our previous studies on BA.2.86 indicated that this lineage is already fully resistant against all therapeutic antibodies that are currently used in the clinics[5] and the same can be assumed for JN.1.

STAR★METHODS

Detailed methods are provided in the online version of this paper and include the following:

- KEY RESOURCES TABLE
- RESOURCE AVAILABILITY
  - Lead contact
  - Materials availability
  - Data and code availability
- EXPERIMENTAL MODEL AND STUDY PARTICIPANT DETAILS
  - Cell culture
  - Plasma samples
- METHOD DETAILS
  - Expression plasmids and sequence analysis
  - Generation of pseudovirus particles and cell entry studies
  - Analysis of pseudovirus particle production and S protein incorporation
  - Analysis of S protein cell surface expression and ACE2 binding efficiency
  - Neutralization assay
- QUANTIFICATION AND STATISTICAL ANALYSIS
- ADDITIONAL RESOURCES

SUPPLEMENTAL INFORMATION

Supplemental information can be found online at https://doi.org/10.1016/j.isci.2024.109904.

ACKNOWLEDGMENTS

We gratefully acknowledge the originating laboratories responsible for obtaining the specimens, as well as the submitting laboratories where the genome data were generated and shared via GISAID, on which this research is based. We further thank Stephan Ludwig, Andrea Maisner, and Gert Zimmer for providing reagents. Finally, we thank the CoCo study participants for their support and the entire CoCo study team for help. S.P. acknowledges funding by the EU project UNDINE (grant agreement number 101057100), the COVID-19-Research Network Lower Saxony (COFONI) through funding from the Ministry for Science and Culture of Lower Saxony (14-76103-184, projects 7FF22, 6FF22, and 10FF22) and the German Research Foundation (Deutsche Forschungsgemeinschaft, DFG; PO 716/11-1). L.Z. acknowledges funding by the China Scholarship Council (CSC) (202006270031). A.D.-J. acknowledges funding by the European Social Fund (ZAM5-87006761) and by

the Ministry for Science and Culture of Lower Saxony (14-76103-184, COFONI Network, project 4LZF23). G.M.N.B. acknowledges funding by German Center for Infection Research (grant no 80018019238), the European Regional Development Funds Defeat Corona (ZW7-8515131) and Getting AIR (ZW7-85151373), and the Ministry for Science and Culture of Lower Saxony (14-76103-184, COFONI Network, project 4LZF23. The funding sources had no role in the design and execution of the study, the writing of the manuscript and the decision to submit the manuscript for publication. The authors did not receive payment by a pharmaceutical company or other agency to write the publication. The authors were not precluded from accessing data in the study, and they accept responsibility to submit for publication.

AUTHOR CONTRIBUTIONS

Conceptualization: L.Z. and M.H.; methodology: S.P. and M.H.; investigation: L.Z., L.G., A.-S.M., and M.H.; formal analysis: L.Z. and M.H.; resources: A.D.-J., A.C., M.V.S., C.F., A.A., S.G.T., and G.M.N.B.; funding acquisition: A.D.-J., G.M.N.B., and S.P.; writing – original draft: M.H.; writing – review & editing: all authors.

DECLARATION OF INTERESTS

S.P. and M.H. conducted contract research (testing of vaccinee sera for neutralizing activity against SARS-CoV-2) for Valneva unrelated to this work. A.D.-J. served as advisor for Pfizer, unrelated to this work. G.M.N.B. served as advisor for Moderna, unrelated to this work. S.P. served as advisor for BioNTech, unrelated to this work.

Received: January 23, 2024
Revised: April 16, 2024
Accepted: May 1, 2024
Published: May 3, 2024

REFERENCES

1. Hu, Y., Zou, J., Kurhade, C., Deng, X., Chang, H.C., Kim, D.K., Shi, P.Y., Ren, P., and Xie, X. (2023). Less neutralization evasion of SARS-CoV-2 BA.2.86 than XBB sublineages and CH.1.1. Emerg. Microbes Infect. *12*, 2271089. https://doi.org/10.1080/22221751.2023.2271089.
2. Uriu, K., Ito, J., Kosugi, Y., Tanaka, Y.L., Mugita, Y., Guo, Z., Hinay, A.A., Jr., Putri, O., Kim, Y., Shimizu, R., et al. (2023). Transmissibility, infectivity, and immune evasion of the SARS-CoV-2 BA.2.86 variant. Lancet Infect. Dis. *23*, e460–e461. https://doi.org/10.1016/S1473-3099(23)00575-3.
3. Yang, S., Yu, Y., Jian, F., Song, W., Yisimayi, A., Chen, X., Xu, Y., Wang, P., Wang, J., Yu, L., et al. (2023). Antigenicity and infectivity characterisation of SARS-CoV-2 BA.2.86. Lancet Infect. Dis. *23*, e457–e459. https://doi.org/10.1016/S1473-3099(23)00573-X.
4. Khan, K., Lustig, G., Römer, C., Reedoy, K., Jule, Z., Karim, F., Ganga, Y., Bernstein, M., Baig, Z., Jackson, L., et al. (2023). Evolution and neutralization escape of the SARS-CoV-2 BA.2.86 subvariant. Nat. Commun. *14*, 8078. https://doi.org/10.1038/s41467-023-43703-3.
5. Zhang, L., Kempf, A., Nehlmeier, I., Cossmann, A., Richter, A., Bdeir, N., Graichen, L., Moldenhauer, A.S., Dopfer-Jablonka, A., Stankov, M.V., et al. (2024). SARS-CoV-2 BA.2.86 enters lung cells and evades neutralizing antibodies with high efficiency. Cell *187*, 596–608.e17. https://doi.org/10.1016/j.cell.2023.12.025.
6. Qu, P., Xu, K., Faraone, J.N., Goodarzi, N., Zheng, Y.M., Carlin, C., Bednash, J.S., Horowitz, J.C., Mallampalli, R.K., Saif, L.J., et al. (2024). Immune evasion, infectivity, and fusogenicity of SARS-CoV-2 BA.2.86 and FLip variants. Cell *187*, 585–595.e6. https://doi.org/10.1016/j.cell.2023.12.026.
7. World Health Organization (2023). Initial Risk Evaluation of JN.1. https://www.who.int/docs/default-source/coronaviruse/18122023_jn.1_ire_clean.pdf?sfvrsn=6103754a_3.
8. Schmidt, F., Weisblum, Y., Muecksch, F., Hoffmann, H.H., Michailidis, E., Lorenzi, J.C.C., Mendoza, P., Rutkowska, M., Bednarski, E., Gaebler, C., et al. (2020). Measuring SARS-CoV-2 neutralizing antibody activity using pseudotyped and chimeric viruses. J. Exp. Med. *217*, e20201181. https://doi.org/10.1084/jem.20201181.
9. Yang, S., Yu, Y., Xu, Y., Jian, F., Song, W., Yisimayi, A., Wang, P., Wang, J., Liu, J., Yu, L., et al. (2024). Fast evolution of SARS-CoV-2 BA.2.86 to JN.1 under heavy immune pressure. Lancet Infect. Dis. *24*, e70–e72. https://doi.org/10.1016/S1473-3099(23)00744-2.
10. Kaku, Y., Okumura, K., Padilla-Blanco, M., Kosugi, Y., Uriu, K., Hinay, A.A., Jr., Chen, L., Plianchaisuk, A., Kobiyama, K., Ishii, K.J., et al. (2024). Virological characteristics of the SARS-CoV-2 JN.1 variant. Lancet Infect. Dis. *24*, e82. https://doi.org/10.1016/S1473-3099(23)00813-7.
11. Planas, D., Staropoli, I., Michel, V., Lemoine, F., Donati, F., Prot, M., Porrot, F., Guivel-Benhassine, F., Jeyarajah, B., Brisebarre, A., et al. (2024). Distinct evolution of SARS-CoV-2 Omicron XBB and BA.2.86/JN.1 lineages combining increased fitness and antibody evasion. Prepritn at. bioRxiv *1*. https://doi.org/10.1101/2023.11.20.567873.
12. Dadonaite, B., Brown, J., McMahon, T.E., Farrell, A.G., Asarnow, D., Stewart, C., Logue, J., Murrell, B., Chu, H.Y., Veesler, D., and Bloom, J.D. (2023). Full-spike deep mutational scanning helps predict the evolutionary success of SARS-CoV-2 clades. Prepritn at. bioRxiv *1*. https://doi.org/10.1101/2023.11.13.566961.
13. Jeworowski, L.M., Muhlemann, B., Walper, F., Schmidt, M.L., Jansen, J., Krumbholz, A., Simon-Loriere, E., Jones, T.C., Corman, V.M., and Drosten, C. (2024). Humoral immune escape by current SARS-CoV-2 variants BA.2.86 and JN.1, December 2023. Euro Surveill. *29*. https://doi.org/10.2807/1560-7917.ES.2024.29.2.2300740.
14. Riepler, L., Rossler, A., Falch, A., Volland, A., Borena, W., von Laer, D., and Kimpel, J. (2020). Comparison of Four SARS-CoV-2 Neutralization Assays. Vaccines (Basel) *9*, 13. https://doi.org/10.3390/vaccines9010013.
15. Aggarwal, A., Fichter, C., Milogiannakis, V., Akerman, A., Ison, T., Silva, M.R., Esneau, C., Bartlett, N., Burrell, L.M., Patel, S.K., et al. (2023). TMPRSS2 activation of Omicron lineage Spike glycoprotein is regulated by TMPRSS2 cleavage of ACE2. Prepritn at. bioRxiv *1*. https://doi.org/10.1101/2023.09.22.558930.
16. Barros-Martins, J., Hammerschmidt, S.I., Cossmann, A., Odak, I., Stankov, M.V., Morillas Ramos, G., Dopfer-Jablonka, A., Heidemann, A., Ritter, C., Friedrichsen, M., et al. (2021). Immune responses against SARS-CoV-2 variants after heterologous and homologous ChAdOx1 nCoV-19/BNT162b2 vaccination. Nat. Med. *27*, 1525–1529. https://doi.org/10.1038/s41591-021-01449-9.
17. Behrens, G.M.N., Cossmann, A., Stankov, M.V., Schulte, B., Streeck, H., Förster, R., Bosnjak, B., Willenzon, S., Boeck, A.L., Thu Tran, A., et al. (2020). Strategic Anti-SARS-CoV-2 Serology Testing in a Low Prevalence Setting: The COVID-19 Contact (CoCo) Study in Healthcare Professionals. Infect. Dis. Ther. *9*, 837–849. https://doi.org/10.1007/s40121-020-00334-1.
18. Hoffmann, M., Kleine-Weber, H., Schroeder, S., Krüger, N., Herrler, T., Erichsen, S., Schiergens, T.S., Herrler, G., Wu, N.H., Nitsche, A., et al. (2020). SARS-CoV-2 Cell Entry Depends on ACE2 and TMPRSS2 and Is Blocked by a Clinically Proven Protease Inhibitor. Cell *181*, 271–280.e8. https://doi.org/10.1016/j.cell.2020.02.052.
19. Brinkmann, C., Hoffmann, M., Lübke, A., Nehlmeier, I., Krämer-Kühl, A., Winkler, M.,

and Pöhlmann, S. (2017). The glycoprotein of vesicular stomatitis virus promotes release of virus-like particles from tetherin-positive cells. PLoS One *12*, e0189073. https://doi.org/10.1371/journal.pone.0189073.

20. Hoffmann, M., Zhang, L., Krüger, N., Graichen, L., Kleine-Weber, H., Hofmann-Winkler, H., Kempf, A., Nessler, S., Riggert, J., Winkler, M.S., et al. (2021). SARS-CoV-2 mutations acquired in mink reduce antibody-mediated neutralization. Cell Rep. *35*, 109017. https://doi.org/10.1016/j.celrep.2021.109017.
21. Hoffmann, M., Arora, P., Groß, R., Seidel, A., Hörnich, B.F., Hahn, A.S., Krüger, N., Graichen, L., Hofmann-Winkler, H., Kempf, A., et al. (2021). SARS-CoV-2 variants B.1.351 and P.1 escape from neutralizing antibodies. Cell *184*, 2384–2393.e12. https://doi.org/10.1016/j.cell.2021.03.036.
22. Hoffmann, M., Arora, P., Nehlmeier, I., Kempf, A., Cossmann, A., Schulz, S.R., Morillas Ramos, G., Manthey, L.A., Jäck, H.M., Behrens, G.M.N., and Pöhlmann, S. (2023). Profound neutralization evasion and augmented host cell entry are hallmarks of the fast-spreading SARS-CoV-2 lineage XBB.1.5. Cell. Mol. Immunol. *20*, 419–422. https://doi.org/10.1038/s41423-023-00988-0.
23. Zhang, L., Kempf, A., Nehlmeier, I., Cossmann, A., Dopfer-Jablonka, A., Stankov, M.V., Schulz, S.R., Jäck, H.M., Behrens, G.M.N., Pöhlmann, S., and Hoffmann, M. (2023). Neutralisation sensitivity of SARS-CoV-2 lineages EG.5.1 and XBB.2.3. Lancet Infect. Dis. *23*, e391–e392. https://doi.org/10.1016/S1473-3099(23)00547-9.
24. Kleine-Weber, H., Elzayat, M.T., Wang, L., Graham, B.S., Müller, M.A., Drosten, C., Pöhlmann, S., and Hoffmann, M. (2019). Mutations in the Spike Protein of Middle East Respiratory Syndrome Coronavirus Transmitted in Korea Increase Resistance to Antibody-Mediated Neutralization. J. Virol. *93*, e013811-18. https://doi.org/10.1128/JVI.01381-18.
25. Berger Rentsch, M., and Zimmer, G. (2011). A vesicular stomatitis virus replicon-based bioassay for the rapid and sensitive determination of multi-species type I interferon. PLoS One *6*, e25858. https://doi.org/10.1371/journal.pone.0025858.
26. Arora, P., Zhang, L., Rocha, C., Sidarovich, A., Kempf, A., Schulz, S., Cossmann, A., Manger, B., Baier, E., Tampe, B., et al. (2022). Comparable neutralisation evasion of SARS-CoV-2 omicron subvariants BA.1, BA.2, and BA.3. Lancet Infect. Dis. *22*, 766–767. https://doi.org/10.1016/S1473-3099(22)00224-9.

STAR★METHODS

KEY RESOURCES TABLE

REAGENT or RESOURCE	SOURCE	IDENTIFIER
Antibodies		
Goat anti-Human IgG (H + L) Cross-Adsorbed Secondary Antibody, Alexa Fluor 488	Thermo Fisher Scientific	Cat# A-11013; RRID:AB_2534080
SARS-CoV/SARS-CoV-2 (COVID-19) spike antibody [1A9], IgG1, Unconjugated, Mouse, Monoclonal	Biozol	Cat# GTX632604; RRID:AB_2864418
Goat anti-Mouse IgG, IgM, IgA (H + L) Secondary Antibody, Alexa Fluor 488	Thermo Fisher Scientific	Cat# A-10667; RRID:AB_2534057
Anti-VSV-M [23H12] Antibody	Kerafast	Cat# EB0011; RRID: AB_2734773
Goat IgG anti-Mouse IgG (H + L)-HRPO	Dianova	Cat# 115-035-003; RRID: AB_10015289
Goat IgG anti-Rabbit IgG (H + L)-HRPO	Dianova	Cat# 111-035-045; RRID: AB_2337938
Anti-VSV-G antibody (I1, produced from CRL-2700 mouse hybridoma cells)	ATCC	Cat# CRL-2700; RRID: CVCL_G654
Bacterial and virus strains		
VSV*ΔG-FLuc	Laboratory of Gert Zimmer	N/A
One Shot™ OmniMAX™ 2 T1R Chemically Competent *E. coli*	Thermo Fisher Scientific	Cat# C854003
Biological samples		
Patient Plasma (10167)	Laboratory of Georg M.N. Behrens	N/A
Patient Plasma (10170)	Laboratory of Georg M.N. Behrens	N/A
Patient Plasma (10172)	Laboratory of Georg M.N. Behrens	N/A
Patient Plasma (10178)	Laboratory of Georg M.N. Behrens	N/A
Patient Plasma (10179)	Laboratory of Georg M.N. Behrens	N/A
Patient Plasma (10180)	Laboratory of Georg M.N. Behrens	N/A
Patient Plasma (10182)	Laboratory of Georg M.N. Behrens	N/A
Patient Plasma (10185)	Laboratory of Georg M.N. Behrens	N/A
Patient Plasma (10186)	Laboratory of Georg M.N. Behrens	N/A
Patient Plasma (10188)	Laboratory of Georg M.N. Behrens	N/A
Patient Plasma (10189)	Laboratory of Georg M.N. Behrens	N/A
Patient Plasma (10191)	Laboratory of Georg M.N. Behrens	N/A
Patient Plasma (10192)	Laboratory of Georg M.N. Behrens	N/A
Patient Plasma (10194)	Laboratory of Georg M.N. Behrens	N/A
Patient Plasma (10197)	Laboratory of Georg M.N. Behrens	N/A
Patient Plasma (10198)	Laboratory of Georg M.N. Behrens	N/A
Patient Plasma (10200)	Laboratory of Georg M.N. Behrens	N/A
Patient Plasma (10201)	Laboratory of Georg M.N. Behrens	N/A
Patient Plasma (10208)	Laboratory of Georg M.N. Behrens	N/A
Patient Plasma (10212)	Laboratory of Georg M.N. Behrens	N/A
Patient Plasma (10214)	Laboratory of Georg M.N. Behrens	N/A
Patient Plasma (10215)	Laboratory of Georg M.N. Behrens	N/A
Patient Plasma (10223)	Laboratory of Georg M.N. Behrens	N/A
Patient Plasma (10224)	Laboratory of Georg M.N. Behrens	N/A

(*Continued on next page*)

Continued

REAGENT or RESOURCE	SOURCE	IDENTIFIER
Chemicals, peptides, and recombinant proteins		
Soluble human ACE2 (sol-hACE2-Fc)	Laboratory of Stefan Pöhlmann	N/A
Critical commercial assays		
Beetle-Juice Kit	PJK	Cat# 102511
Experimental models: cell lines		
293T	DSMZ	Cat# ACC-635; RRID: CVCL_0063
Calu-3	Laboratory of Stephan Ludwig	ATCC Cat# HTB-55; RRID: CVCL_0609
Vero	Laboratory of Andrea Maisner	ATCC Cat# CRL-1587; RRID: CVCL_0603
Vero E6-TMPRSS2	Laboratory of Stuart G. Turville	CellBank Australia Cat# JCRB1819; RRID: CVCL_YQ49
Vero E6-ACE2+TMPRSS2	Laboratory of Stuart G. Turville	N/A
Oligonucleotides		
SARS-2-S Seq-01 (CAAGATCTACAGCAAGCACAC)	Sigma-Aldrich	N/A
SARS-2-S Seq-02 (GTCGGCGGCAACTACAATTAC)	Sigma-Aldrich	N/A
SARS-2-S Seq-03 (GCTGTCTGATCGGAGCCGAG)	Sigma-Aldrich	N/A
SARS-2-S Seq-04 (TGAGATGATCGCCCAGTACAC)	Sigma-Aldrich	N/A
SARS-2-S Seq-05 (GCCATCTGCCACGACGGCAAAG)	Sigma-Aldrich	N/A
pCG1 F (CCTGGGCAACGTGCTGGT)	Sigma-Aldrich	N/A
pCG1 R (GTCAGATGCTCAAGGGGCTTCA)	Sigma-Aldrich	N/A
EG.5.1-S Seq-02 (GCGGCAACTACAATTACCTG)	Sigma-Aldrich	N/A
EG.5.1-S Seq-03 (CGGCTGTCTGATCGGAGCCGAG)	Sigma-Aldrich	N/A
BA.2.86-S Seq-02 (AAACACAGCGGCAACTACG ATTACTGG)	Sigma-Aldrich	N/A
BA.2.86-S Seq-03 (CTGTCTGATCGGAGCCGAGTACG)	Sigma-Aldrich	N/A
XBB.1.5 (L455F + F456L) R (GTCCCGCTCGAAG GGCTTCAG CTTGGACTTCCGCAAGAACCGGTACAGGTAAT TGTAGTTGC)	Sigma-Aldrich	N/A
XBB.1.5 (A475V) F (CTGAAGCCCTTCGAGCGGGA CATCTCCACCGAGATCTATCAGGtCGGCAaCAag CCTTGTAACG)	Sigma-Aldrich	N/A
EG.5.1 (F157L) R (GCTGTACACCCGCAGCTCGCTTT CCATCCAGCTCTTG)	Sigma-Aldrich	N/A
EG.5.1 (F157L) F (GATGGAAAGCGAGCTGCGGGT GTACAGCAGCGCCAAC)	Sigma-Aldrich	N/A
EG.5.1 (L452R) R (CAACAGCCGGTACCGGTAATT GTAGTTGCCGCTG)	Sigma-Aldrich	N/A
EG.5.1 (L452R) F (CTACAATTACCGGTACCGGCT GTTGCGGAAGTC)	Sigma-Aldrich	N/A
XBB.2.3 (N185D) R (GGTTCTTGAAGTCGCCCTCCT TGCCTTCCAGG)	Sigma-Aldrich	N/A
XBB.2.3 (N185D) F (GGAAGGCAAGGAGGGCGACTT CAAGAACCTGCGCGAG)	Sigma-Aldrich	N/A
XBB.2.3 (T478R) R (CCGTTACAAGGCCGGTTGCCGGCCTGATAGATCTC)	Sigma-Aldrich	N/A
XBB.2.3 (T478R) F (CAGGCCGGCAACCGGCCTTG TAACGGCGTAGC)	Sigma-Aldrich	N/A

(*Continued on next page*)

Continued

REAGENT or RESOURCE	SOURCE	IDENTIFIER
BA.2.86 (L455S) R (GGACTTCCGGAAGGACCGGTAC CAGTAATCGTAGTTGC)	Sigma-Aldrich	N/A
BA.2.86 (L455S) F (GATTACTGGTACCGGTCCTTCCG GAAGTCCAAGCTGAAG)	Sigma-Aldrich	N/A
Recombinant DNA		
Plasmid: pCG1	Laboratory of Roberto Cattaneo	N/A
Plasmid: pCAGGS-VSV-G	Laboratory of Stefan Pöhlmann	N/A
Plasmid: pCAGGS-DsRed	Laboratory of Stefan Pöhlmann	N/A
Plasmid: pCG1-SARS-2-SΔ18 (B.1), codon-optimized	Laboratory of Stefan Pöhlmann	N/A
SARS-2-SΔ18 (XBB.1.5), codon-optimized	Laboratory of Stefan Pöhlmann	N/A
SARS-2-SΔ18 (EG.5.1), codon-optimized	Laboratory of Stefan Pöhlmann	N/A
Plasmid: pCG1-SARS-2-SΔ18 (BA.2.86), codon-optimized	Laboratory of Stefan Pöhlmann	N/A
Plasmid: pCG1-SARS-2-SΔ18 (JD.1.1), codon-optimized	This study	N/A
Plasmid: pCG1-SARS-2-SΔ18 (HV.1), codon-optimized	This study	N/A
Plasmid: pCG1-SARS-2-SΔ18 (GS.4.1), codon-optimized	This study	N/A
Plasmid: pCG1-SARS-2-SΔ18 (JN.1), codon-optimized	This study	N/A
Plasmid: pCG1_solACE2-Fc	Laboratory of Stefan Pöhlmann	N/A
Software and algorithms		
Hidex Sense Microplate Reader Software	Hidex Deutschland Vertrieb GmbH	https://www.hidex.de
ID7000 Spectral Cell Analyzer Software (version 1.1.8.18211)	Sony Biotechnology	https://www.sonybiotechnology.com/
Adobe Photoshop CS5 Extended (version 12.0 × 32)	Adobe	https://www.adobe.com/
GraphPad Prism (version 8.3.0(538))	GraphPad Software	https://www.graphpad.com/
Microsoft Office Standard 2010 (version 14.0.7232.5000)	Microsoft Corporation	https://products.office.com/
ImageJ (version 1.54days)	U. S. National Institutes of Health, Bethesda, Maryland, USA	https://imagej.net/ij/index.html
Other		
Information on SARS-CoV-2 lineage frequency and mutations	Cov-Spectrum database	https://cov-spectrum.org/

RESOURCE AVAILABILITY

Lead contact

Requests for material can be directed to Stefan Pöhlmann (spoehlmann@dpz.eu) and the lead contact Markus Hoffmann (mhoffmann@dpz.eu).

Materials availability

All materials and reagents will be made available upon installment of a material transfer agreement.

Data and code availability

All data reported in this paper will be shared by the lead contact upon request. This paper does not report original code. Any additional information required to reanalyze the data reported in this paper is available from the lead contact upon request.

EXPERIMENTAL MODEL AND STUDY PARTICIPANT DETAILS

Cell culture

Vero (African green monkey kidney, female, kidney; CRL-1586, ATCC; RRID: CVCL 0574, kindly provided by Andrea Maisner), 293T (human, female, kidney; ACC-635, DSMZ; RRID: CVCL 0063), Vero E6 cells stably expressing TMPRSS2 (Vero-TMPRSS2; JCRB1819, CellBank Australia; RRID: CVCL_YQ49), and Vero E6 cells stably expressing ACE2 and TMPRSS2 (Vero-ACE2+TMPRSS2)[15] were cultivated using

Dulbecco's modified Eagle medium (DMEM, PAN-Biotech), supplemented with 10% fetal bovine serum (Biochrom), 100 U/ml of penicillin, and 0.1 mg/mL of streptomycin (PAN-Biotech). Calu-3 cells (human, male, lung; HTB-55, ATCC; RRID: CVCL_0609, kindly provided by Stephan Ludwig) were cultivated using DMEM/F-12 medium (GIBCO), supplemented with 10% fetal bovine serum (Biochrom), 100 U/ml penicillin and 0.1 mg/mL streptomycin (PAN-Biotech), 1x non-essential amino acid solution (from 100x stock, PAN-Biotech) and 1 mM sodium pyruvate (PAN-Biotech). All cell lines were incubated at 37°C in a humidified atmosphere containing 5% CO_2 and regularly tested for the absence of mycoplasma contamination. Cell lines were further validated by STR analysis, partial sequencing of the cytochrome *c* oxidase gene, microscopic examination, and/or according to their growth characteristics. Transfection of 293T cells was performed by calcium phosphate precipitation.

Plasma samples

Information on individual plasma samples is provided in Table S1. SARS-CoV-2 S1-specific IgG were quantified using the anti-SARS-CoV-2-QuantiVac-ELISA (IgG) (EUROIMMUN). Further, SARS-CoV-2 infection-free history of cohort 1 was confirmed by absence of anti-SARS-CoV-2 NCP IgG using the anti-SARS-CoV-2 ELISA (NCP) (EUROIMMUN). In total, plasma samples derived from two cohorts were tested and all samples were collected within three weeks following the last vaccination: *cohort 1*, vaccinated individuals without history of SARS-CoV-2 infection who received the XBB.1.5-adapted booster vaccine as last vaccination (n = 11; age range 25–74 (median = 48 years); male to female ratio 4:7); *cohort 2*, vaccinated individuals with history of SARS-CoV-2 infection who received the XBB.1.5-adapted booster vaccine as last vaccination (n = 13; age range 29–62 (median = 44 years); male to female ratio 6:7). All plasma samples were heat-inactivated (56°C, 30 min) prior to their use in neutralization assays. All plasma samples were collected as part of the COVID-19 Contact (CoCo) Study (German Clinical Trial Registry, DRKS00021152), which is a prospective observational study monitoring anti-SARS-CoV-2 IgG and immune responses in health care professionals at Hannover Medical School and individuals with potential contact to SARS-CoV-2.[16,17] The CoCo Study and the analysis performed for this study were approved by the Internal Review Board of Hannover Medical School (institutional review board no. 8973_BO-K_2020, last amendment Sep 2023). All study participants provided written informed consent and received no compensation.

METHOD DETAILS

Expression plasmids and sequence analysis

All information on S protein sequences and SARS-CoV-2 lineages was obtained from GISAID (Global Initiative on Sharing All Influenza Data) (https://gisaid.org/) and CoV-Spectrum (https://cov-spectrum.org/) databases. Expression plasmids pCAGGS-DsRed,[18] pCAGGS-VSV-G,[19] pCG1-sol-ACE2-Fc,[20] pCG1-SARS-CoV-2 B.1 SΔ18 (codon-optimized, C-terminal truncation of 18 amino acid residues, GISAID Accession ID: EPI_ISL_425259),[21] pCG1-SARS-CoV-2 XBB.1.5 SΔ18 (codon-optimized, C-terminal truncation of 18 amino acid residues, GISAID Accession ID: EPI_ISL_16239158),[22] pCG1-SARS-CoV-2 EG.5.1 SΔ18 (codon-optimized, C-terminal truncation of 18 amino acid residues, GISAID Accession ID: EPI_ISL_18095879),[23] and pCG1-SARS-CoV-2 BA.2.86.1 SΔ18 (codon-optimized, C-terminal truncation of 18 amino acid residues, GISAID Accession ID: EPI_ISL_18114953)[5] have been described before. The expression plasmid for SARS-CoV-2 JD.1.1 SΔ18 (GISAID Accession ID: EPI_ISL_18501311) was generated by introduction of mutations L455F, F456L, and A475V into plasmid pCG1-SARS-CoV-2 XBB.1.5 SΔ18 by overlap-extension PCR, while the expression plasmid for SARS-CoV-2 HV.1 SΔ18 (GISAID Accession ID: EPI_ISL_18285095) was generated by introduction of mutations F157L and L452R into plasmid pCG1-SARS-CoV-2 EG.5.1 SΔ18 by overlap-extension PCR. In addition, the expression plasmid for SARS-CoV-2 JN.1 SΔ18 (GISAID Accession ID: EPI_ISL_18530042) was generated by introduction of mutation L455S into plasmid pCG1-SARS-CoV-2 BA.2.86.1 SΔ18 by overlap-extension PCR, while the expression plasmid for SARS-CoV-2 GS.4.1 SΔ18 (GISAID Accession ID: EPI_ISL_18536879) was generated by introduction of mutations N185D and T478R into plasmid pCG1-SARS-CoV-2 XBB.2.3 SΔ18[23] by overlap-extension PCR. All full-length S protein open-reading frames generated by overlap-extension PCR were inserted into the pCG1 expression plasmid (kindly provided by Roberto Cattaneo), making use of BamHI and XbaI restriction sites. A commercial sequencing service (Microsynth SeqLab) was used to confirm the integrity of all S protein sequences.

Generation of pseudovirus particles and cell entry studies

The generation of vesicular stomatitis virus-based pseudovirus particles bearing SARS-CoV-2 S proteins and cell entry studies were conducted in accordance to previously published protocol.[24] At 24 h post transfection, 293T cells expressing the respective S protein, VSV-G or dsRed (negative control) were inoculated with VSV-G-transcomplemented VSV*ΔG(FLuc) (kindly provided by Gert Zimmer)[25] and incubated for 1 h at 37°C and 5% CO_2. Subsequently, the inoculum was aspirated and the cells were washed with phosphate-buffered saline (PBS), before cell culture medium with anti-VSV-G antibody (culture supernatant from I1-hybridoma cells; ATCC no. CRL-2700) was added. Of note, cells expressing VSV-G received cell culture medium without antibody. At 16–18 h post inoculation, the culture supernatants were collected, centrifuged to remove cellular debris (4,000 × g, 10 min), and clarified supernatants were aliquoted and stored at −80°C until further use. For cell entry studies, target cells were grown in 96-well plates to 50–90% confluence before they were inoculated with identical volumes of the respective pseudovirus particles and incubated for 16–18 h at 37°C and 5% CO_2. Then, cell entry efficiency was assessed through measurement of virus-encoded luciferase activity in cell lysates. Cells were incubated for 30 min at room temperature with PBS containing 0.5% Tergitol (Carl Roth). Next, lysates were transferred to white 96-well plates, mixed with luciferase substrate (Beetle-Juice, PJK), and luminescence was measured with a Hidex Sense plate luminometer (Hidex).

Analysis of pseudovirus particle production and S protein incorporation

For analysis of S protein particle incorporation, 1 mL of supernatant containing pseudotype particles was concentrated by high-speed centrifugation (13,300 rpm, 90 min, 4°C) through a sucrose cushion (20% w/v sucrose in PBS), before being lysed by addition of 1 volume of 2× sample buffer (0.03 M Tris-HCl, 10% glycerol, 2% SDS, 5% beta-mercaptoethanol, 0.2% bromophenol blue, 1 mM EDTA) and incubation at 96°C for 15 min. Next, the samples were subjected to SDS-PAGE, proteins were blotted onto nitrocellulose membranes (Hartenstein) and membranes were blocked in 5% BSA for 30 min. Membranes were further incubated with primary antibodies overnight at 4°C. Next, membranes were washed three times with PBS-T and subsequently incubated with horseradish peroxidase-coupled secondary antibodies for 1 h at 4°C. Finally, membranes were washed three times with PBS-T, incubated with a home-made chemiluminescence solution (0.1 M Tris-HCl [pH 8.6], 250 g/mL luminol, 0.1 mg/mL *para*-hydroxycoumaric acid, 0.3 percent hydrogen peroxide) and signals were recorded using the ChemoCam imaging system along with the ChemoStar Professional software (Intas Science Imaging Instruments). For detection of S proteins, a primary antibody reactive against the S2 subunit was used (SARS-CoV-2 (2019-nCoV) Spike S2 Antibody; dilution: 1:2000 in PBS/5% BSA; Biozol, Cat: SIN-40590-T62) in combination with a horseradish peroxidase-coupled goat IgG anti-rabbit secondary antibody (dilution: 1:2000 in PBS/5% BSA; Dianova, Cat: 111-035-045). For detection of the loading control vesicular stomatitis virus matrix protein (VSV-M) a primary antibody reactive against VSV-M was used (anti-VSV-M [23H12] antibody; dilution: 1:1000 in PBS/5% skim milk; Kerafast, Cat: EB0011) in combination with a horseradish peroxidase-coupled anti-mouse secondary antibody (dilution: 1:2000 in PBS/5% skim milk; Dianova, Cat: 115-035-003). Quantification of protein bands was performed using the ImageJ software (version 1.54days).

Analysis of S protein cell surface expression and ACE2 binding efficiency

At 24 h post seeding, 293T cells were transfected with expression plasmids for the SARS-CoV-2 S protein or empty vector (control). The next day, cells were washed with PBS and further incubated with fresh culture medium at 37°C and 5% CO_2. At 48 h post transfection, the culture medium was aspirated and cells were washed once with PBS, before they were resuspended in PBS-B (PBS containing 1% bovine serum albumin [BSA; Carl Roth]) and pelleted by centrifugation (600 × g, 5 min, room temperature). After removal of the supernatant, the cell pellet was resuspended in 500 µL PBS-B and each sample was split into two tubes. Following pelleting of the cells (600 × g, 5 min, room temperature) and removal of the supernatant, one of the two tubes for each sample was used for the detection of S protein cell surface expression, while the other tube was used for ACE2 binding studies. (i) Analysis of S protein cell surface expression: Cell pellets were resuspended in 250 µL PBS-B containing anti-SARS-CoV-2 S2 subunit antibody (mouse, 1:100; GTX632604, Biozol) and incubated for 1 h at 4°C using a Rotospin test tube rotator disk (IKA). Next, cells were pelleted (600 × g, 5 min, room temperature), washed once with PBS-B, resuspended in 250 µL PBS-B containing Alexa Fluor-488-conjugated anti-mouse antibody (1:200; Thermo Fisher Scientific, A-10667) and incubated for 1 h at 4°C using a Rotospin test tube rotator disk. Afterward, cells were pelleted (600 × g, 5 min, room temperature), washed twice with PBS-B, resuspended in 250 µL 1% paraformaldehyde solution for fixation (30 min, room temperature). Thereafter, cells were pelleted, washed with PBS-B, pelleted again and resuspended in 100 µL PBS-B, before S protein cell surface expression was analyzed using an ID7000 Spectral Cell Analyzer along with the ID7000 software (Sony Biotechnology, San Jose, CA, USA). (ii) Analysis of ACE2 binding: Cell pellets were resuspended in 250 µL PBS-B containing solACE2-Fc (soluble human ACE2 ectodomain fused to the Fc portion of human immunoglobulin G [IgG]; 20× concentrated supernatant of 293T cells transfected with pCG1-sol-ACE2-Fc; 1:20) and incubated for 1 h at 4°C using a Rotospin test tube rotator disk. Next, cells were pelleted (600 × g, 5 min, room temperature), washed once with PBS-B, resuspended in 250 µL PBS-B containing Alexa Fluor-488-conjugated anti-human antibody (1:200; Thermo Fisher Scientific, A-11013) and incubated for 1 h at 4°C using a Rotospin test tube rotator disk. Afterward, cells were pelleted (600 × g, 5 min, room temperature), washed twice with PBS-B, resuspended in 250 µL 1% paraformaldehyde solution for fixation (30 min, room temperature). Thereafter, cells were pelleted, washed with PBS-B, pelleted again and resuspended in 100 µL PBS-B, before ACE2 binding was analyzed using an ID7000 Spectral Cell Analyzer along with the ID7000 software (Sony Biotechnology, San Jose, CA, USA). In order to adjust ACE2 binding efficiency for differences in surface expression between the different S proteins, S protein cell surface expression was first normalized against the S protein of the SARS-CoV-2 B.1 lineage (set as 1) and the resulting quotient was used to correct the respective ACE2 binding data.

Neutralization assay

Neutralization assays were conducted in accordance with a previously published protocol.[26] First, S protein-bearing pseudovirus particles were incubated with different dilutions of blood plasma (dilution range: 1:25 or 1:6,400) for 30 min at 37°C and subsequently inoculated onto confluent Vero cell monolayers. At 16–18 h post inoculation, neutralization efficiency was assessed by determining the relative inhibition of pseudovirus entry in the presence of plasma compared to pseudovirus entry in the absence of plasma (reference, 0% inhibition). Next, a non-linear regression model was used to calculate the plasma dilution leading to half-maximal inhibition (neutralizing titer 50, NT50) for each plasma/pseudovirus combination. Only NT50 value of 6.25 (25% of lowest plasma dilution tested) or higher were considered positive. Furthermore, relative changes in neutralization (relative to $B.1_{pp}$) were determined. For this, individual fold reduction values for each plasma sample were calculated, and the median value was determined.

QUANTIFICATION AND STATISTICAL ANALYSIS

Data were analyzed with Microsoft Excel (part of Microsoft Office Professional Plus, version 2016, Microsoft Corporation) and GraphPad Prism version 8.3.0 (GraphPad Software). Statistical significance was analyzed by two-way analysis of variance with Tukey's multiple comparison test

(cell entry, ACE2 binding) or Friedmann test with Dunn's multiple comparison test (plasma neutralization). Statistical significance was considered for adjusted p values of 0.05 or lower (ns [not significant], $p > 0.05$; *, $p \leq 0.05$; **, $p \leq 0.01$; ***, $p \leq 0.001$).

ADDITIONAL RESOURCES

Plasma samples were collected as part of the COVID-19 Contact (CoCo) Study (German Clinical Trial Registry, DRKS00021152), which is a prospective observational study monitoring anti-SARS-CoV-2 IgG and immune responses in health care professionals at Hannover Medical School and individuals with potential contact to SARS-CoV-2 (https://drks.de/search/en/trial/DRKS00021152). The CoCo Study and the analysis performed for this study were approved by the Internal Review Board of Hannover Medical School (institutional review board no. 8973_BO-K_2020, last amendment Sep 2023).